J. Biochem. 2009;145(4)505–515
doi:10.1093/jb/mvp002

Cooperative Binding of L-Trp to Human Tryptophan 2,3-Dioxygenase: Resonance Raman Spectroscopic Analysis

Eiko Fukumura[1,2], Hiroshi Sugimoto[1,*], Yuko Misumi[3], Takashi Ogura[3,4] and Yoshitsugu Shiro[1]

[1]Biometal Science Laboratory, RIKEN SPring-8 Center, Harima Institute, 1-1-1 Kouto, Sayo, Hyogo; [2]Department of Biological Sciences, Graduate School of Science, Osaka University, 1-1 Machikaneyama-cho, Toyonaka, Osaka; [3]Department of Life Science; and [4]Picobiology Institute, Graduate School of Life Science, University of Hyogo, Koto 3-2-1, Kamigori-cho, Ako-gun, Hyogo, Japan

Received November 8, 2008; accepted January 6, 2009; published online January 17, 2009

Tryptophan 2,3-dioxygenase (TDO) is a tetrameric enzyme that catalyses the oxidative cleavage of L-tryptophan (L-Trp) to *N*-formylkynurenine by the addition of O_2 across the 2,3-bond of the indole ring. This reaction is the first and rate-limiting step in the kynurenine pathway in mammals. In the present study, we measured the conformational changes in the haem pocket of recombinant human TDO (rhTDO) in ferric form that are induced by L-Trp binding using both resonance Raman and optical absorption spectroscopies. The deconvolution analysis of the haem Raman bands at various concentrations of L-Trp revealed that the wild-type enzyme exhibits homotropic cooperativity in L-Trp binding, which was confirmed by a change in the optical absorption spectra. Mutation analysis showed that the Y42F mutant abolished the cooperative binding, and that the H76A mutant considerably reduced the catalytic activity. These data and the inter-subunit contacts reported in the bacterial TDO structure suggest that the Y42 of rhTDO is responsible for the cooperative binding of L-Trp by participating in the active site of the adjacent subunit.

Key words: heam, allosteric regulation, tryptophan, Raman spectra.

Abbreviations: CT1, charge transfer band; IDO, indoleamine 2,3-dioxygenase; L-Trp, L-tryptophan; Mb, myoglobin; rhTDO, recombinant human TDO; TDO, tryptophan 2,3-dioxygenase; xTDO, *Xanthomonas campestris* TDO.

INTRODUCTION

Oxygenases (*1*) are metal- or flavin-containing enzymes that catalyse the direct incorporation of molecular oxygen (O_2) atom(s) into substrates (*2*). There are two types of oxygenases: monooxygenases add one oxygen atom, and dioxygenases insert both atoms of molecular oxygen. To date, only tryptophan 2,3-dioxygenase (TDO) and indoleamine 2,3-dioxygenase (IDO) have been identified as haem-containing dioxygenases (*3*), both of which can catalyse conversion of L-tryptophan (L-Trp) to *N*-formylkynurenine (*4*). The enzymatic reaction is the first and rate-limiting step in the major metabolic pathway of L-Trp.

In mammals, IDO is only present as a monomeric enzyme, and it is ubiquitously distributed in all tissues except for the liver (*5*, *6*). This enzyme is inducible by interferon-γ, and, thus, is highly involved in immune function (*6–10*). In contrast, TDO, which shares no sequence homology with IDO, is widely distributed across species, ranging from bacteria to mammals, as a homo-tetrameric enzyme (*9*, *11*, *12*). In mammals, TDO is mainly present in the liver, but, recently, the enzyme was detected in the brain, epidermis, spermatozoa, placenta, and so on (*13–16*). Unlike IDO, which exhibits broad substrate specificity for the indoleamines, the activity of TDO is specific for L-Trp (*9*, *17*, *18*). TDO is induced by glucocorticoid hormones and is also regulated by the availability of the physiological substrate, L-Trp (*19*, *20*).

TDO has been known as an allosteric enzyme (*2*); TDO isolated from *Xanthomonas pruni* shows sigmoidal kinetics and its activity is inhibited by intermediates of the NAD biosynthetic pathway (*21*). Its cooperativity is enhanced by anthranilic acid and is diminished by α-methyl Trp. Early studies of rat liver TDO also showed that NADPH and 3-hydroxy anthranilate are negative modulators of TDO activity (*22*, *23*). These data indicate that TDO is regulated by feedback control and that the enzyme has multiple binding sites. However, the mechanism of substrate regulation (i.e. homotropic allosteric modulation) is not well understood. Recent crystallographic analysis of recombinant *Xanthomonas campestris* TDO (xTDO) revealed two L-Trp-binding sites and extensive interaction between the subunits of the tetramer. Although the TDO structure suggests that it has a cooperative mechanism, there is no direct evidence for homotropic cooperative binding of L-Trp to xTDO, as the measurement of the dioxygenase activity reveals Michaelis–Menten-type kinetics.

Herein, we demonstrate the cooperative binding of L-Trp to recombinant human TDO (rhTDO) by analysis of conformational changes in the haem using resonance Raman spectroscopy. In addition, mutation analysis also

*To whom correspondence should be addressed: Tel: +81-791-58-2817, Fax: +81-791-58-2818, E-mail: sugimoto@spring8.or.jp

provides insight into roles of key residues in the activity of the enzyme.

MATERIALS AND METHODS

Construction of Expression Plasmid—Human tryptophan 2,3-dioxygenase (hTDO) cDNA (Image clone 4071714) in the pDNR-LIB vector was purchased from American Type Culture Collection. First, we constructed, expressed, and purified full-length hTDO. N-terminal sequence analysis of the purified full-length hTDO revealed that it was truncated at the N-terminal end, with loss of up to 15 amino-acid residues. Thus, we constructed rhTDO, and deleted the 15 residues at the N-terminus. The hTDO cDNA was amplified by PCR using a forward primer (5′-GGG CATATG AAAAAACT CCCCGTAGAAGG-3′), which encodes an *Nde*I site (underlined), followed by the coding sequence starting at Met connected to K16, and a reverse primer (5′-GGGG ATCCTTAATCTGATTCATCACTG CTGAAGTAGG-3′), which contains the coding sequence up to the termination codon, followed by an *BamHI* site (underlined). This amplified fragment was directly ligated to *Nde*I/*Bam*HI-digested pET15b with a hexa-histidine tag and a thrombin site fused to the N-terminus of hTDO-ΔN15, to produce pET15b hTDO-ΔN15. Two other mutants (H76A, Y42F) were prepared using the QuikChange site-directed mutagenesis kit (Stratagene) with pET15b hTDO-ΔN15 as a template. Plasmids containing pET15b hTDO-ΔN15 and the mutants were used to transform *Esherichia coli* DH5α cells. All constructs were verified by DNA sequencing.

Expression of Recombinant Human TDO—*Esherichia coli* Rosetta (DE3) pLysS cells were transformed using the plasmid construct. Single colonies on LB-agar plates containing ampicillin (100 μg/ml) and chloramphenicol (70 μg/ml) were selected, and the cells were grown overnight at 37°C in 2 ml of LB medium containing 100 μg/ml of ampicillin and 70 μg/ml chloramphenicol. The overnight culture (0.5 ml of culture) was used to inoculate 2 l of TB medium (yeast extract, 24.0 g/l; polypeptone, 12.0 g/l; glycerol, 0.4% w/v; KH_2PO_4, 2.31 g/l; and, K_2HPO_4, 12.5 g/l) supplemented with 100 μg/ml ampicillin, 70 μg/ml chloramphenicol, 0.5 mM δ-aminolevulinic acid and 0.2 mM Fe_2SO_4. The cultures were grown in TB medium until $OD_{600} = 1.1–1.3$, and protein expression was induced with 0.5 mM IPTG. The cells were then cultured for ~20 h at 30°C, followed by centrifugation at $10,000 \times g$ for 10 min at 4°C The cell pellets were stored at −80°C until they were used for protein purification.

Purification of Recombinant Human TDO—Frozen cell pellets were resuspended in 120 ml of lysis buffer [50 mM potassium phosphate (pH 8.0), i.e. buffer A] containing EDTA-free complete protease inhibitor cocktail tablets (Roche), lysozyme (0.1 mg/ml), and DNaseI (0.01 mg/ml), followed by stirring for 1 h. Cells were lysed by sonication, and the cell debris was removed by ultracentrifugation at $185,000 \times g$ for 30 min at 4°C. The resulting supernatant was loaded onto a Ni-NTA agarose (Qiagen) column that had been equilibrated with lysis buffer supplemented with 300 mM NaCl (buffer B). The column was washed with the same buffer containing 50 mM imidazole (buffer C), and His-tagged proteins were eluted from the column using the same buffer containing 300 mM imidazole (buffer D). The His tags were cleaved by direct addition of biotinylated thrombin (Novagen) to the elutant, which was then dialysed against buffer B overnight at 4°C. The thrombin-treated protein solution was then loaded onto a Ni–NTA column that had been equilibrated with buffer B. After an additional wash with buffer A, cleaved rhTDO was separated from the uncleaved His-tagged proteins by elution with buffer C. The eluted protein was concentrated and further purified using a Superdex-200 size-exclusion column with buffer A containing 200 mM NaCl (buffer E). The fractions that contained molecules similar in size to tetrameric hTDO were pooled, and concentrated using Amicon Ultra-15 centrifugal filter devices (Millipore) containing a cellulose filter with a 50 kDa cutoff. After concentration of the fractions, the solution was filtered with a 0.22 μm disposable filter. The concentration of the purified recombinant hTDO was estimated using the pyridine haemochrome assay (*24*, *25*). The haem *b* extinction coefficient used in this study was $\varepsilon_{557}-\varepsilon_{541} = 20.7\ mM^{-1}cm^{-1}$ (*26*). The concentrated sample was flash-frozen in liquid nitrogen, and stored at −80°C until further use.

Enzyme Assay—The activity of ferric hTDO was measured in buffer E at 37°C under normal atmospheric conditions. The rate of *N*-formylkynurenine formation was monitored at 321 nm ($\varepsilon = 3{,}750\ M^{-1}cm^{-1}$) (*27*). The reaction was initiated by the addition of ferric rhTDO, and after the small lag phase, the linear velocity was measured. The enzyme concentration was 0.5 μM in a final volume of 2.0 ml. During the measurements, the reaction medium was gently stirred in a cuvette with a 1 cm light path. The kinetic data were fitted to the Michaelis–Menten equation using IGOR Pro 5.05 software (WaveMetrics, Inc.).

Raman Spectroscopy—The purified rhTDO, buffer E, and buffer E containing 5 mM L-Trp were each dispensed into small glass vials. Each vial was sealed with a rubber stopper and an open-top screw cap. All vials were deoxygenated by repeated evacuation and flushing with N_2 gas. To establish strictly anaerobic conditions, the de-aerated vials were passed into an anaerobic glove box ($O_2 < 5$ ppm), where they were kept for at least 12 h at 4°C. Samples with an enzyme concentration of 300 μM (75 μM of tetramer) and various concentrations of L-Trp were prepared in the glove box using these stock solutions. For measurements of the Raman spectra, the sample solutions were put into a cylindrical quartz cell with a small magnetic stir bar, and the cell was secured with a rubber septum.

Raman scattering was excited at 413.1 nm using a Kr ion laser (Spectra Physics). The Raman scattered light passed through a depolarizer and the entrance slit of a 1.0 m monochromator equipped with a 1,200 groove per millimetre ruled grating blazed at 500 nm (MC-100DG, Ritsu Ohyo Kogaku Co., Ltd). The detector was a 1,100 × 330 pixel, back-illuminated, liquid nitrogen-cooled charge-coupled device detector (LN/CCD-1100PB, Roper Scientific). The entrance slit-width of the monochromator was set at 250 μm. The cylindrical cell was spun at 1,200 rpm to minimize local heating.

A holographic notch filter was used to eliminate Rayleigh scattering. The frequency calibration of the spectrometer was performed with indene as the standard. The laser power was maintained at 300 μW for all measurements. The acquisition time was 30 min for all of the spectra obtained. Winspec/32 software (Roper Scientific) was used for data acquisition. Spectral analysis was performed using IGOR Pro5.05 (WaveMetrics, Inc.). After subtracting the best-fit linear baseline from the data, the Gaussian function was used in the fitting procedure for multiple overlapping peaks. Gaussian fitting and peak area calculations were carried out using the Igor Pro multi-peak fitting package.

UV-visible Absorption Spectroscopy—The protein solutions used for the measurement of absorption spectra were prepared by the same protocol as in Raman experiments. The protein and L-Trp solutions were mixed into the quartz cell with a screw cap and the desired concentration in an anaerobic glove box. The UV-visible region of absorption spectra was measured with an enzyme concentration of 4 μM in the absence and presence of 5 mM L-Trp at 20°C under a N_2 atmosphere. The absorption change in the visible region (530–700 nm) by L-Trp titration was measured with 240 μM of enzyme by the addition of a small volume of 50 mM L-Trp to the enzyme in the glove box. All experiments of optical absorption spectra were performed using a Hitachi U-3000 spectrophotometer equipped with a thermoelectric cell holder and an SPR-10 temperature controller. The temperature of the spectrometer was controlled at 20°C using a water bath (Lauda thermostat RM6).

RESULTS

Design of Mutation—As shown in Fig. 1, crystallographic analysis of xTDO revealed that the interaction of xTDO with L-Trp involves the H-bond between H55 and the N1 atom of L-Trp. This observation suggests that the role of H55 in the catalytic activity of the enzyme might be the abstraction of a proton due to the basic nature of the amino acid (*11*). However, the residual activity (15% in k_{cat}) of the H55A mutant suggests another possibility for the roles of this residue in the catalytic reaction, which is still a matter of debate (*28*). On the other hand, the residue of the adjacent subunit in the xTDO structure, Y24, participates in the formation of the active site and interacts with the 4-vinyl group and the indole ring of L-Trp by hydrophobic interaction. The key residues in the catalytic site of xTDO, H55 and Y24, are conserved in hTDO as H76 and Y42, respectively (Supplementary Fig. S1). We prepared two mutants of rhTDO (H76A and Y42F) and characterized their enzymatic and spectroscopic properties.

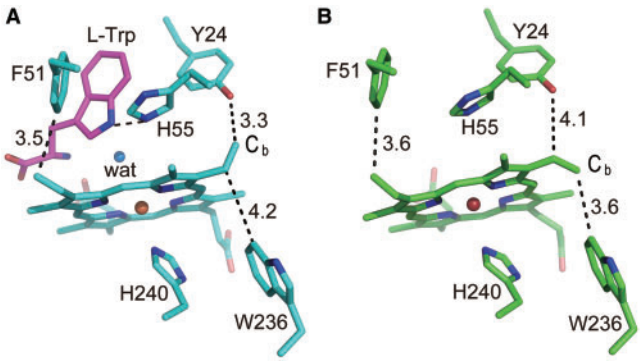

Fig. 1. **Active site of *Xanthomonas campestris* TDO.** (A) substrate-bound and (B) substrate-free forms are depicted as ball-and-stick models, with the carbon atoms shown in cyan and green, respectively. The carbon atoms of the substrate, L-Trp, are shown in magenta. Oxygen, nitrogen and iron atoms are shown in red, blue and brown, respectively. The conformation of the 4-vinyl group of the haem differs significantly between the substrate-bound and -free forms. The C_b atom interacts with Y24 in the L-Trp bound form, but with W236 in the free form. Figures were prepared with the PyMOL program (*36*) using PDB codes 2NW7 and 2NW8.

Activity of Ferric hTDO—The enzymatic activities of wild-type rhTDO, and of the Y42F and H76A mutants in the ferric state, were measured using various concentrations of the substrate, L-Trp. Previous studies have demonstrated that the ferric enzyme has the capability to degrade L-Trp (*29*). The rate of the product formation under open-air conditions (~400 μM) was plotted against the applied L-Trp concentration, as shown in Fig. 2. The plot was fitted with the Michaelis–Menten equation, providing the apparent kinetic parameters [$K_{m(app)}$, $k_{cat(app)}$], that is compiled in Table 1. Since the separate experiment shows that the activity reaches saturation at an oxygen concentration of ~60 μM (data not shown), the $K_{m(app)}$ and $k_{cat(app)}$ values appear to be close to the true K_m and k_{cat} values. The obtained $K_{m(app)}$ of wild-type (82.5 μM) is comparable to the L-Trp concentration found in the liver of rats with normal diets (40–90 μmol/kg liver) (*30*). As shown by the values of $k_{cat(app)}/K_{m(app)}$, the enzymatic activity of rhTDO was reduced to 3% and 0.1% in the Y42F and H76A mutants, respectively. This result

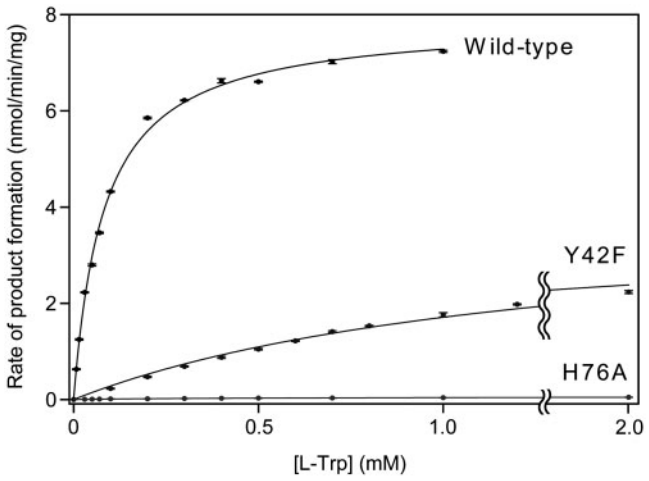

Fig. 2. **Rate of product formation *versus* substrate concentration.** Initial reaction rate of wild-type rhTDO, and of the H76A and Y42F mutants plotted as a function of L-Trp. Each value is the mean of three replicates with error bars representing the standard deviation of each sampling point. Kinetic parameters were estimated by fitting the data to the standard Michaelis–Menten equation and are shown in Table 1. The reaction experiments were performed with an enzyme concentration of 0.5 μM, at 37°C, in 50 mM potassium phosphate buffer, pH 8.0.

Table 1. **Apparent kinetic parameters for oxidation of L-Trp by ferric rhTDO and its mutants.**

	rhTDO (pH 7.0)[a]	rhTDO (pH 8.0)	H76A (pH 8.0)	Y42F (pH 8.0)
$K_{m(app)}$ (μM)	180	82.5 ± 3.8	488 ± 51	1,290 ± 140
$k_{cat(app)}$ (s^{-1})	0.6	6.12 ± 0.02	0.04 ± 0.00	3.04 ± 0.04
$k_{cat(app)}/K_{m(app)}$	3×10^{-3}	7.42×10^{-2}	9×10^{-5}	2.36×10^{-3}

Experiments were performed with an enzyme concentration of 0.5 μM, at 37°C, in 50 mM potassium phosphate buffer, pH 8.0. It should be noted that these rates were determined under normal atmospheric conditions. [a]Batabyal, D. and Yeh, S. R. published results.

suggests that both residues make significant contributions to the enzymatic reaction of rhTDO. In the case of the Y42F mutation, the change in $K_{m(app)}$ is mainly responsible for the loss of enzymatic activity, while both $K_{m(app)}$ and $k_{cat(app)}$ are significantly reduced in the H76A mutation.

Raman Spectra of the Wild-Type Enzyme—Figure 3 shows the resonance Raman spectra of ferric rhTDO in the presence of 0–1 mM of L-Trp. The assignments of the bands, which are described in the spectra, were based on those of ferric Mb (*31*) and rhTDO, as previously reported (*29*). In the high frequency region of the substrate-free enzyme [Fig. 3A(a)], the positions of the ν_4 (1,372 cm^{-1}), ν_3 (1,482 cm^{-1}) and ν_2 (1,560 cm^{-1}) bands are essentially identical to those of the corresponding bands of haemoproteins in the six-coordinate high-spin state.

Raman spectral changes were observed upon the addition of L-Trp. In the high-frequency region (Fig. 3A), the ν_4 band shifted slightly from 1,372 to 1,374 cm^{-1}, and the ν_3 band appeared at ~1,505 cm^{-1}, suggesting an appearance of the haem iron in the six-coordinate, low-spin state. The reduction of the ν_2 peak intensity at 1,560 cm^{-1} is indicative of a six-coordinate, high-spin/low-spin mixture (*32*). In the low-frequency region (Fig. 3B), the intensity of the γ_6 (pyrrole tilting mode) band at 338 cm^{-1} was reduced, while that of the ν_8 vibration (in-plane skeletal mode) at 350 cm^{-1} increased with the L-Trp concentration. The intensity of the haem propionate bending mode, $\delta(C_\beta C_c C_d)_{6,7}$ at 378 cm^{-1} and 391 cm^{-1}, decreased. The intensity of the haem 4-vinyl bending mode, $\delta(C_\beta C_a C_b)_4$, at 416 cm^{-1}, decreased, although the 2-vinyl bending mode, $\delta(C_\beta C_a C_b)_2$, at 430 cm^{-1}, did not change. The decrease in the intensity of the vinyl stretching mode, ν_{cc}, at 1,625 cm^{-1}, also supports a conformational change in the vinyl group. Because the vinyl stretching vibration, ν_{cc}, and the in-plane skeletal mode, ν_{10}, can overlap at 1,625 cm^{-1}, we measured the polarized resonance Raman spectra of ferric rhTDO (Supplementary Fig. S2) to determine the depolarization ratio of the Raman band. From the spectra, the polarization ratio of the band at 1,625 cm^{-1} was calculated to be 0.25 and 0.24 in both the absence and presence of L-Trp, respectively. Because the polarization ratio is expected to be 0 and ~0.75 for the ν_{cc} and ν_{10} modes, respectively, the results show that the ν_{cc} band is the major contributor to the intensity change at 1,625 cm^{-1}.

We analysed the Raman bands in the 250–450 cm^{-1} region by fitting the data with Gaussian curves.

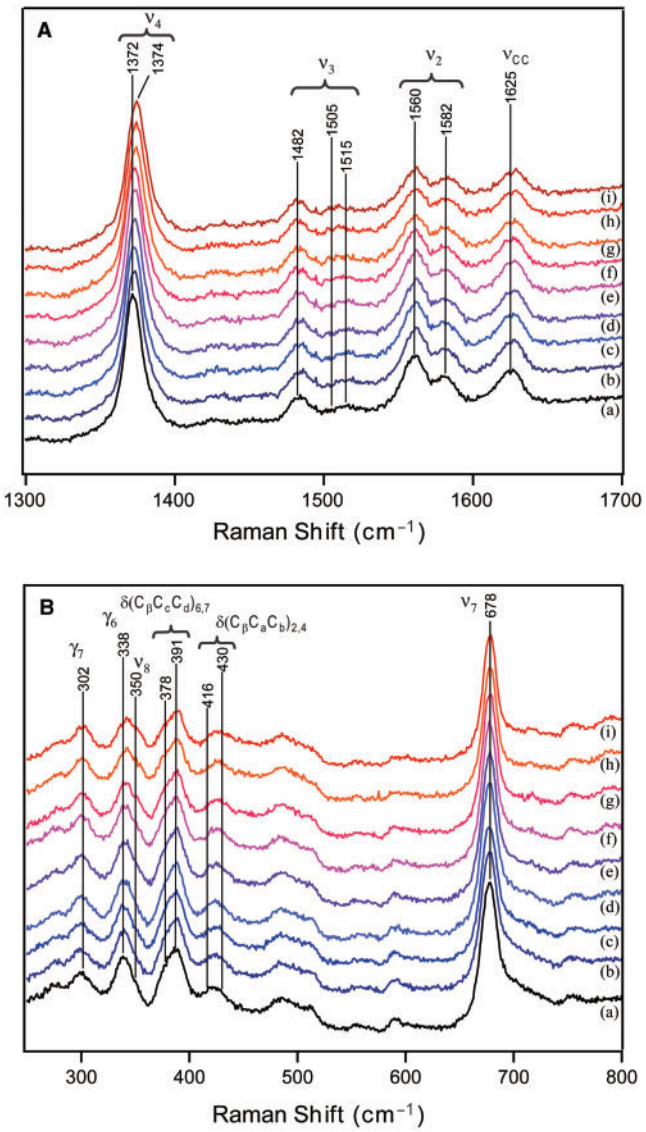

Fig. 3. **Resonance Raman spectra of wild-type rhTDO for various L-Trp concentrations.** (A) High-frequency and (B) low-frequency regions are shown. The measurement conditions were as follows: (a) ferric rhTDO without L-Trp, (b) ferric rhTDO + 50 μM L-Trp, (c) ferric rhTDO + 100 μM L-Trp, (d) ferric rhTDO + 200 μM L-Trp, (e) ferric rhTDO + 300 μM L-Trp, (f) ferric rhTDO + 400 μM L-Trp, (g) ferric rhTDO + 600 μM L-Trp, (h) ferric rhTDO + 800 μM L-Trp, (i) ferric rhTDO + 1 mM L-Trp.

As illustrated in Fig. 4A, the deconvolution allowed us to identify nine well-resolved peaks and to detect changes in the intensity of the γ_6, ν_8, $\delta(C_\beta C_c C_d)$ at 378 cm^{-1} and $\delta(C_\beta C_a C_b)_4$ bands. In this analysis, we used the peak area as an indicator of peak intensity. Because the ν_7 mode at 678 cm^{-1} is not significantly affected by either the spin or oxidation states, its intensity was used as a reference to scale the intensity of other modes in each spectrum. The relative intensity of each band was plotted as a function of the L-Trp concentration, as shown in Fig. 5. The plots clearly show the sigmoidal shape for the wild-type rhTDO. Because these conformational changes in the haem reflect the binding of L-Trp to the

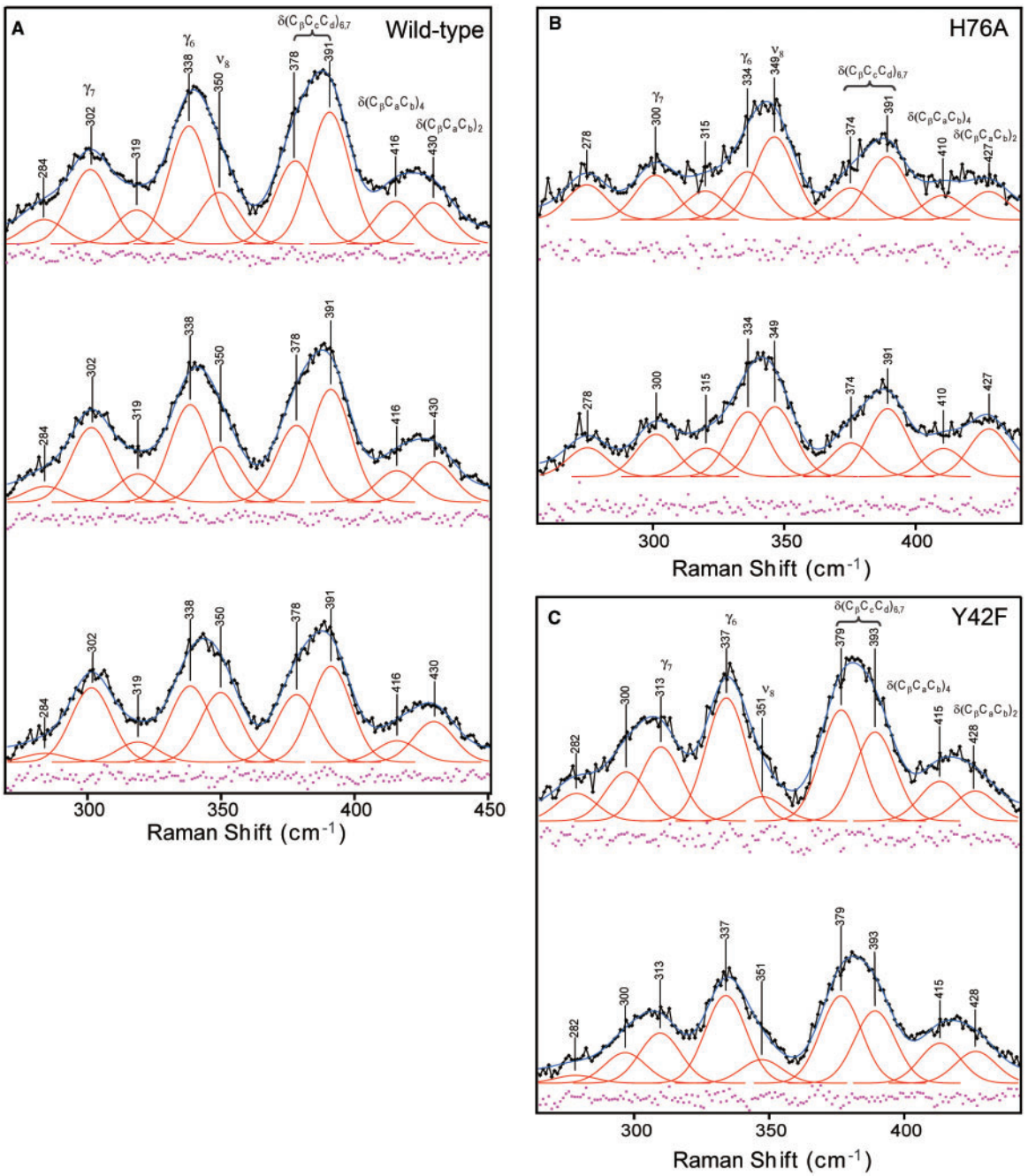

Fig. 4. **Deconvolution analysis of Raman bands in the low-frequency region.** (A) ferric rhTDO (top), ferric rhTDO + 400 μM L-Trp (middle) and ferric rhTDO + 1 mM L-Trp (bottom), (B) ferric H76A mutant (top) and ferric H76A mutant + 2 mM L-Trp (bottom), (C) ferric Y42F mutant (top) and ferric Y42F mutant + 2 mM L-Trp (bottom). The black line with the filled rectangle represents the experimental data. The blue line superimposed on the experimental data represents the calculated data. The nine peaks shown in red are the result of the deconvolution analysis. The dots at the bottom of each spectrum are the residuals from the peak-fitting calculation.

catalytic sites, the sigmoidal curves imply that the haem conformational change exhibits an allosteric response. The sigmoidicity parameter (Hill coefficient) were estimated as 2.4, 2.7, 2.5 and 2.3 for the γ_6, ν_8, $\delta(C_\beta C_c C_d)$ at 378 cm^{-1} and $\delta(C_\beta C_a C_b)_4$ modes, respectively.

Absorption Spectra of Wild-Type rhTDO—The absorption maxima in the optical absorption spectra of the wild-type rhTDO in ferric form, measured at pH 8.0, are shown in Fig. 6A. A Soret maximum was observed at 405 nm, α/β bands were observed at 585/504 nm, and a charge transfer band (CT1) was observed at 632 nm. These characteristics are consistent with the spectral features of haem proteins in the ferric, high-spin state (*26*). Upon addition of the substrate, L-Trp, the spectrum

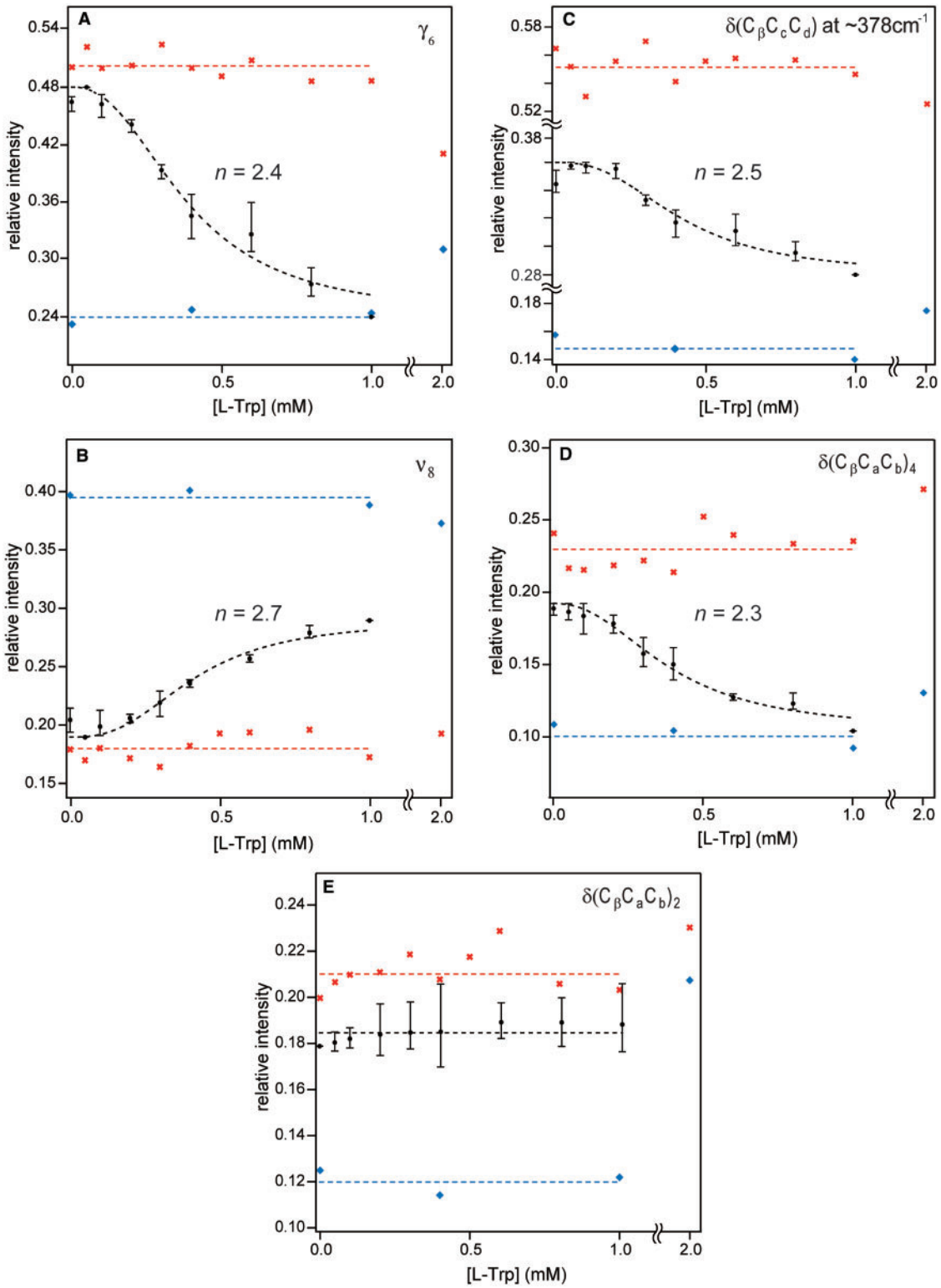

Fig. 5. **Plot of the intensity *versus* L-Trp concentration.** The intensities of (A) γ_6,(B) ν_8, (C) $\delta(C_\beta C_c C_d)$ at ~378 cm^{-1}, (D) $\delta(C_\beta C_a C_b)_4$, (E) $\delta(C_\beta C_a C_b)_2$ modes are plotted for the wild-type (filled circle in black), Y42F mutant (cross in red), H76A mutant (diamond in blue). The vertical axis is the ratio of target intensity to the intensity of the ν_7 mode. Each plotted value for the wild-type is the mean of triplicate measurements and the error bars indicate minimum and maximum values of three replicates. The dashed lines for the wild-type enzyme are the best-fit curves calculated using Hill equation. Each value plotted for the mutants represents a single measurement. The dashed lines for the mutants indicate the mean of values in 0–1 mM L-Trp.

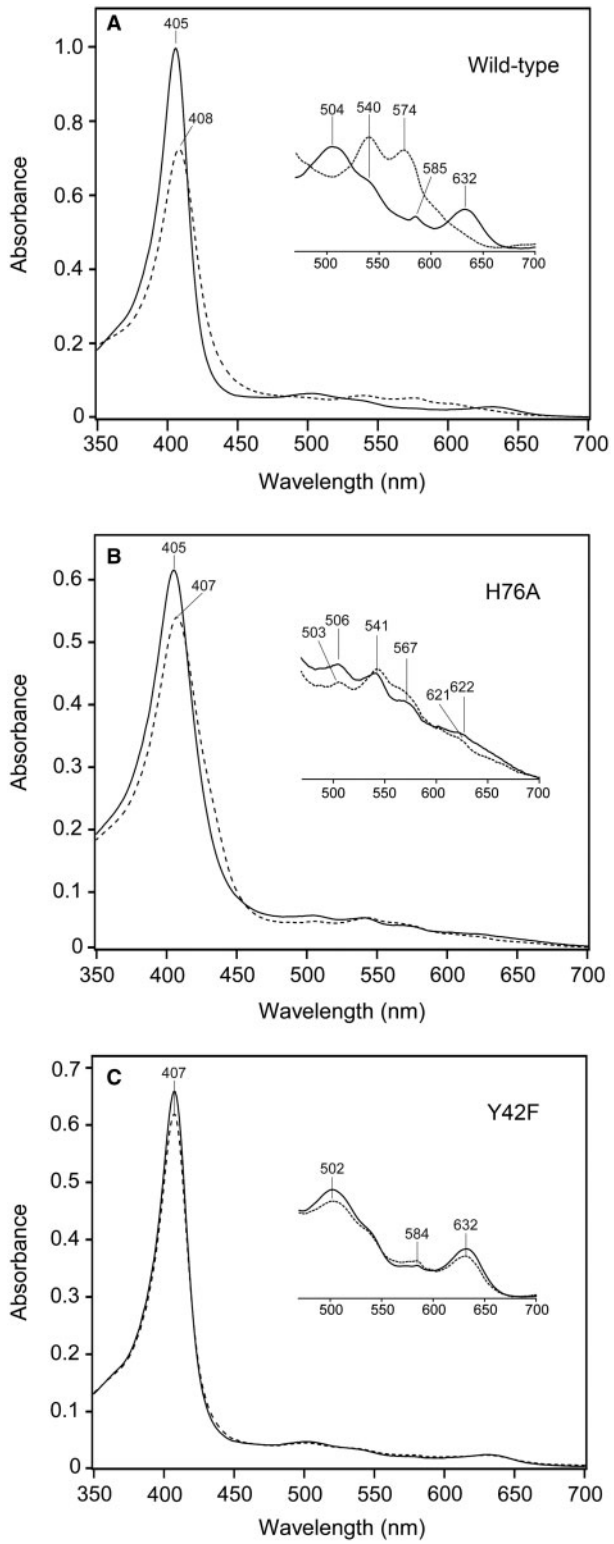

Fig. 6. **Absorption spectra of rhTDO and its mutants.** (A) Spectra of wild-type rhTDO, (B) H76A mutant and (C) Y42 mutant in the absence (solid line) and presence (dotted line) of 5 mM L-Trp. Solutions were prepared with 4 μM enzyme in 50 mM potassium phosphate (pH 8.0) under anaerobic conditions. The inset is the expanded view of the visible bands.

was significantly altered: the Soret maximum was red-shifted from 405 to 408 nm, new α/β bands appeared at 574 and 540 nm, and CT1 band was reduced, but did not completely disappear (Fig. 7A). The spectral change was attributed to a mixture of the low- and high-spin states in haem iron after binding of the L-Trp to rhTDO, which is consistent with the results of Raman experiments.

The sigmoidal kinetics of L-Trp binding observed in Raman spectral change is supported by the absorption spectral change, as shown in Fig. 7B. The Hill coefficients estimated from the intensity of 632 and 574 nm are 3.3 and 3.2, respectively. These values are slightly larger than those estimated from Raman spectra, mostly because the data point was extended to a higher concentration of L-Trp in the measurement of the absorption spectra.

Raman Spectra of the H76A Mutant—In the high-frequency region of the ferric substrate-free form of the H76A mutant (Supplementary Fig. S3), the ν_3 band appeared at 1,481 and ~1,507 cm^{-1}, which implies that it adopts a six-coordinate and the high-spin/low-spin mixture, in contrast to the high-spin state of the substrate-free wild-type enzyme. The ν_4 band was slightly down-shifted from 1,373 to 1,372 cm^{-1} by the mutation. As in the wild-type enzyme, the deconvolution analysis of the 250–450 cm^{-1} region showed nine peaks (Fig. 4B). Because the spin state of ferric H76A in the substrate-free form is different from that of the wild-type, the positions and the intensities of these Raman bands are different. Furthermore, H76A does not show an apparent spin transition upon L-Trp binding, and the mutation considerably reduces the affinity for L-Trp, as supported by a 6-fold increase in the $K_{m(app)}$ value. Therefore, the intensities of ν_8, $\delta(C_\beta C_c C_d)_{6,7}$ and $\delta(C_\beta C_a C_b)_4$ do not change significantly upon the addition (0–2 mM) of L-Trp (Fig. 5B–D). A small increase in the intensity of both γ_6 vibration at 334 cm^{-1} and $\delta(C_\beta C_a C_b)_2$ vibration at 427 cm^{-1} was detected only when 2 mM L-Trp was used (Fig. 5A and E). The intensity changes of these Raman bands do not indicate sigmoidal kinetics.

Absorption Spectra of the H76A Mutant—In the absorption spectrum of the ferric H76A mutant, the Soret band was coincident with the position of the Soret band in the wild-type enzyme, while the CT1 band was shifted from 632 nm to 622 nm in the mutant (Fig. 6B). The resultant spectral features are characteristic of the mixture of high- and low-spin haem irons. It is worth noting that the spectral change in rhTDO induced by the H76A mutation appears similar to the change in the myoglobin (Mb) spectrum induced by the V68D mutation (*33*). The effect of the Mb mutation has been explained by changes in the electrostatic interaction of the haem distal pocket with residue 68. Binding of L-Trp to the ferric H76A mutant leads to a red-shift in the Soret band (from 405 to 407 nm), and a blue-shift in the high-spin β band (from 506 to 503 nm), indicating that L-Trp binding to the active site of the H76A mutant affects both the π–π^* transitions and porphyrin skeletal vibrations. The intensity changes of these bands were too small to conduct a quantitative analysis.

Raman Spectra of the Y42F Mutant—In the high-frequency region of Raman spectra for the ferric

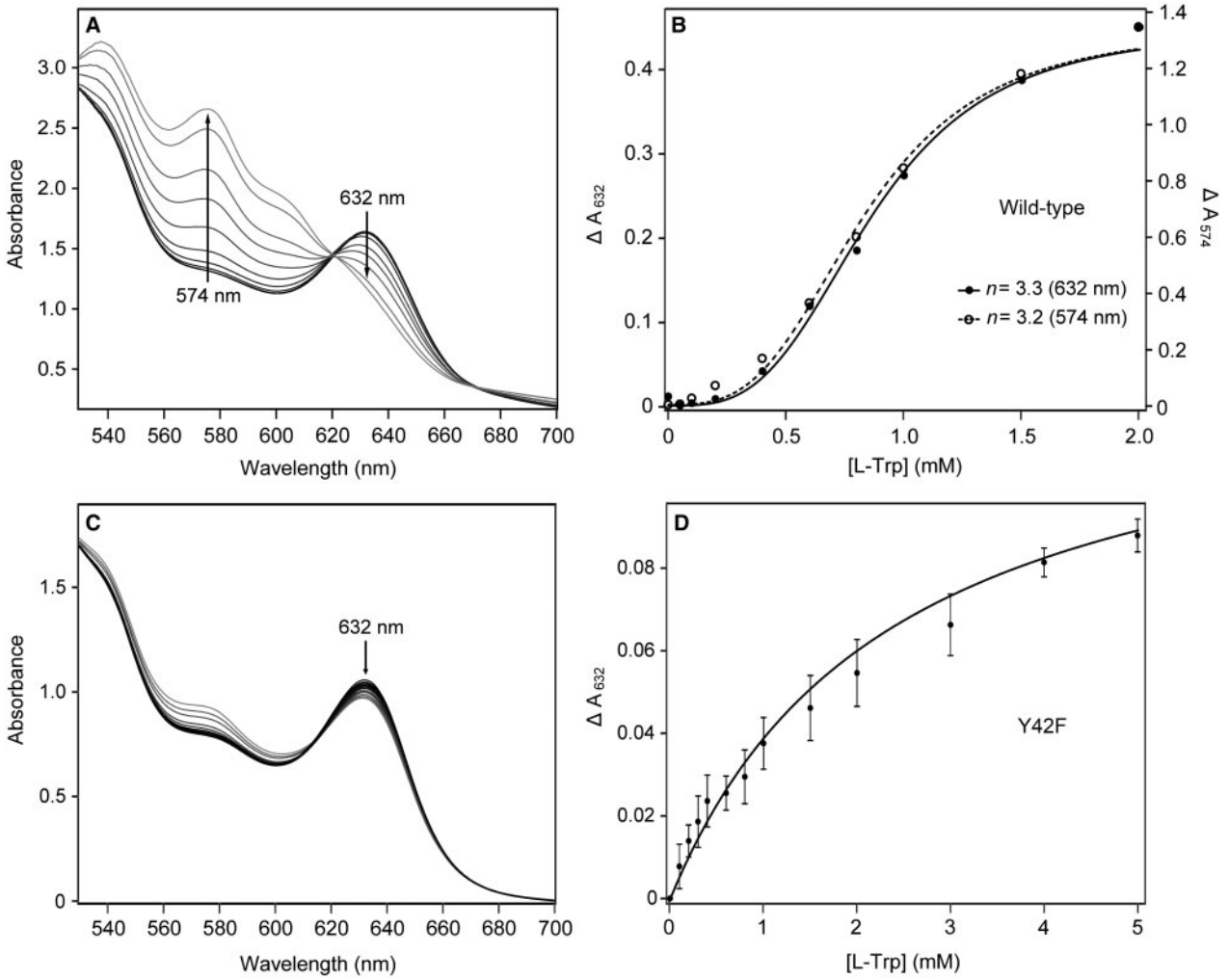

Fig. 7. **Change of absorption spectra by the addition of L-Trp.** (A) The visible region of absorption spectra of wild-type enzyme upon successive additions of L-Trp. (B) The intensity of the CT1 band at 632 nm (filled circle) α band at 574 nm (circle) in (A) are plotted as a function of L-Trp concentration, and fitted to the Hill equation (solid and dashed line, respectively). (C) The visible region of the absorption spectra of the Y42F mutant upon successive additions of L-Trp. (D) The intensity of the CT1 band at 632 nm in (C) are plotted and fitted to the Michaelis-Menten equation (solid line).

substrate-free form of Y42F (Supplementary Fig. S3), the intensity of the ν_2 band at ~1,557 cm^{-1}, relative to that of 1,576 cm^{-1}, is similar to that of wild-type, which implies that the Y42F mutant predominantly adopts the six-coordinate, high-spin state. After addition of L-Trp, the ν_4 band was slightly down-shifted from 1,372 to 1,371 cm^{-1}, unlike the pattern observed for the wild-type and H76A mutant enzymes. Despite the greater enzyme activity of the Y42F mutant relative to the H76A mutant, addition of L-Trp at concentrations up to 2 mM did not affect most bands in the 250–450 cm^{-1} region, except for a slight reduction in the γ_6 peak, as shown in Fig. 4C and 5A–E. The binding of L-Trp has a very small effect on the spin-state of the haem iron. These results are consistent with the 16-fold increase in the $K_{m(app)}$ value (Table 1).

Absorption Spectra of the Y42F Mutant—The absorption spectrum of the Y42F mutant shows the Soret band at 407 nm, α/β bands at 584/502 nm, and the CT1 band at 632 nm (Fig. 6C), This spectrum pattern is similar to that of a wild-type in the absence of L-Trp. The red-shift of the Soret band by 2 nm upon the mutation of Y42F implies that the π–π^* transitions of the porphyrin ring are affected by the removal of the OH group. The L-Trp binding to the Y42F mutant alters only the intensity of the absorption bands. The plot of the intensity of the CT1 band of the Y42F mutant exhibits simple saturation kinetics (Fig. 7C and D), which is in sharp contrast to the sigmoidal behavior of a wild-type enzyme (Fig. 7B).

DISCUSSION

L-Tryptophan Binding to rhTDO—The analysis of substrate binding to ferric rhTDO using resonance Raman spectroscopy has been reported by Batabyal and Yeh (*29*), who compared the spectra of the substrate (L-Trp)-free and -bound enzymes. These results were essentially reproduced in the present study, as shown in Fig. 3. In the present study, we carefully examined the

spectral changes of the ferric enzyme during the titration of the substrate, L-Trp. We quantified changes in the peak intensities using deconvolution analysis, which resolved the γ_6 (338 cm^{-1}), ν_8 (350 cm^{-1}), $\delta(C_\beta C_c C_d)_{6,7}$ (378, 391 cm^{-1}) and $\delta(C_\beta C_a C_b)_4$ (416 cm^{-1}) bands in all spectra.

The intensities of the out-of-plane γ_6 mode and the in-plane skeletal ν_8 mode are sensitive to the distortion of the haem plane. Because the Fe atoms are out of the haem plane in the high-spin state, but are in-plane for the low-spin state atoms (*31*), the change of the γ_6 and ν_8 intensities of wild-type rhTDO reflects the mixing the low- to high-spin states upon the L-Trp binding. This result is consistent with the optical spectral data described above. The mixed-spin state indicates that binding of L-Trp to ferric hTDO might facilitate deprotonation of the water that is bound to the sixth coordination position of the haem iron.

Because the haem propionate bending modes, $\delta(C_\beta C_c C_d)_{6,7}$, are sensitive to their environment, the change in their intensity with the elevation of the L-Trp concentration indicates altered H-bonding interactions of the haem propionates upon the L-Trp binding. In addition, the haem 4-vinyl bending mode, $\delta(C_\beta C_a C_b)_4$, which was well-resolved from the 2-vinyl bending mode, $\delta(C_\beta C_a C_b)_2$, in our analysis, decreased in its intensity upon the L-Trp binding, suggesting a reduction in π-conjugation of the vinyl group with the porphyrin π-system (*34*). A similar change was not observed in the 2-vinyl bending mode of haem. This result suggests that L-Trp binding induces a conformational change only in the 4-vinyl group of the haem.

The conformational changes in the haem of rhTDO induced by the L-Trp binding can be explained on the basis of the crystal structures of bacterial TDO (xTDO), which is homologous to the human enzyme. One of the most striking differences between the substrate-free and L-Trp-bound xTDO was observed at both the 4-vinyl and 7-propionate groups of haem (Fig. 1). In the substrate-free form, the 4-vinyl group is in the in-plane configuration relative to the porphyrin plane, while it adopts the out-of-plane orientation in the substrate-bound form of xTDO. In addition, the bound L-Trp interacts with the 7-propionate group of the haem via its amino group.

With respect to protein interactions, Y24 of xTDO is involved in hydrophobic interactions with the substrate. In addition, the Y24 hydroxyl group has an OH-π interaction with the 4-vinyl group of the porphyrin (Fig. 1), while the OH group of Y24 is displaced toward the C_b atom of the haem 4-vinyl group by 0.7 Å in the L-Trp-bound form. A similar interaction can be expected in rhTDO. The interaction between the conserved Y42 of hTDO and the 4-vinyl group of the haem might be altered by L-Trp binding, causing the haem 4-vinyl group to rotate, thereby altering the intensity of $\delta(C_\beta C_a C_b)_4$ in the Raman spectra. The importance of this interaction for substrate recognition and the haem environment was confirmed by the Y42F mutation that shows considerably lower affinity for L-Trp and only small changes in the optical spectra and Raman band upon addition of L-Trp.

Allosteric Interaction—A novel finding of the present study using spectroscopic methods is that L-Trp binding to rhTDO is sigmoidal, suggesting homotropic allosteric interaction between the subunits of the tetrameric enzymes. By contrast, the enzymatic activity in various L-Trp concentration exhibits simple saturation with Michaelis–Menten kinetics, because further steps (i.e. the iron reduction and oxygen binding) are required for the reaction. The anaerobic condition in the titration experiments prevents activation of the enzyme. Activation or later step would limit the overall reaction rate.

Reportedly, NADPH is an allosteric inhibitor of rat liver TDO, which implies the existence of feedback control, as TDO catalyses the first step in the kynurenine pathway, leading to the formation of NAD (*22*). The compounds, 3-hydroxy anthranilate and α-methyl Trp, which are not substrates for TDO, are also known as heterotropic allosteric modulators (*23*). On the other hand, the study of homotropic allosteric control in mammalian TDO has been limited to the early work of Schutz *et al.* (*23*), which showed that cooperative kinetics (Hill coefficient of 1.6) of rat liver TDO were observed only at pH 6.2 and were dependent on both the concentration of L-Trp and the presence of α-methyl Trp. These data indicate that mammalian TDO possesses two binding sites—a catalytic site and a regulatory site (*2*). Since previous kinetic studies of rat liver TDO and bacterial TDO were based on the rate of product formation in a steady state, it is unknown which step is cooperative and which is rate limiting. On the other hand, the present study demonstrates that the first step of the reaction, L-Trp binding, is a cooperative manner. Although the physiological significance of our results remains to be elucidated, the reaction steps of hTDO in the liver has the potential for regulation by allosteric interaction involving both homotropic and heterotropic mechanisms.

Although the tertiary structure of hTDO remains to be determined, the crystallographic analysis of xTDO might help to reveal the mechanism of cooperativity. The crystal structure of xTDO complexed with L-Trp reveals that two monomers are tightly packed into the asymmetric unit (*11*). The physiological tetramer results from association with the neighboring dimer, which is related by crystallographic 2-fold symmetry. The interface between the monomers within the internal dimer is formed by the anti-parallel association of the α2 helices (Fig. 8). The helix α3 of xTDO contributes residues F51 and H55 to the formation of the substrate-binding pocket in the distal region of the haem molecule. Interestingly, both the α1 and α2 helices of xTDO are distal to the core of the polypeptide chain and associate with adjacent subunits in the dimer. In particular, α1 provides Y24 for creation of the substrate-binding pocket in another chain. Because the amino-acid sequence in the region of helices α1, α2 and α3 in TDO is highly conserved among all species (Supplementary Fig. S1), it can be assumed that TDOs share a common inter-subunit interaction that allows formation of the tetramer. However, whether binding of L-Trp to the catalytic site can regulate the affinity of another catalytic site remains to be determined. We prepared the Y42F mutant of rhTDO to confirm the role of the conserved Tyr residue that forms the catalytic site of the adjacent subunit. As we expected, the Y42F mutant exhibits considerably lower affinity and catalytic activity than the wild-type enzyme.

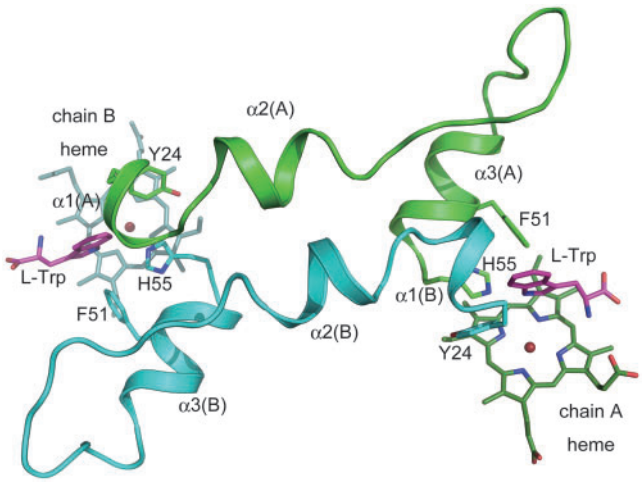

Fig. 8. **Interaction of N-terminal helices with adjacent subunit in the tetrameric structure of xTDO.** The structures of the A and B chains are indicated in green and cyan, respectively. The substrate L-Trp is shown in magenta. Y24 of the A chain interacts with the haem in the B chain. Conversely, Y24 in chain B interacts with haem in chain A.

Furthermore, the Y42F mutant abolished the cooperative binding of L-Trp. These data suggest that Y42 is involved in substrate binding in the catalytic site and is responsible for the transmission of the structural change of one active site to an adjacent subunit.

The Reaction Mechanism of Ferric hTDO—As described above, H55 of xTDO and H76 of hTDO play crucial roles in substrate binding, but the role of these residues in catalysis remains to be controversial. Tong and co-workers have suggested that H55 in xTDO is not essential for catalysis, based on results of their biochemical analysis. They found that the $k_{cat(app)}$ of TDO is insensitive to pH over the range examined (pH 6–8), and the H55A mutant retained 15% of wild-type activity (*11*, *28*). On the other hand, Dick and co-workers showed that mutation of this conserved His in recombinant rat TDO significantly reduced the enzymatic activity (*35*). In the present study, we describe the effect of the H76A mutation on the kinetics of hTDO and discuss in detail the importance of the haem environment. The optical absorption spectra and the high-frequency region of the Raman spectra show that the H76A mutant exhibits an increase in the six-coordinate, low-spin state in the ferric form, whereas the ferric wild-type enzyme mostly exists in the six-coordinate, high-spin state. Thus, H76 is involved, either directly or indirectly, in the regulation of the spin state. Additionally, H76 affects the electrostatic field of the haem pocket, as evidenced by the distinctly different CT1 band of the H76A mutant compared with that of the wild-type enzyme.

Although the H76A mutant has only 0.1% of wild-type activity, its $K_{m(app)}$ value is less than that of the Y42F mutant, which has greater activity than H76A. The shift in the optical absorption spectrum and the ν_4 Raman band of H76A after the addition of L-Trp also indicates that the L-Trp-binding ability is not fully lost in the H76 mutant. Based on the comparison with bacterial TDO structures, it is likely that H76 of hTDO interacts with the hydrogen of the N1 atom of L-Trp in the catalytic site. Although the present study did not provide direct evidence that H76 acts as a catalytic base for abstraction of a proton from L-Trp, we conclude that H76 of hTDO is important for substrate binding in the haem pocket as well as for the catalytic reaction.

The rhTDO has a novel characteristic, in which no reducing agent is required for ferric iron to be reduced to its ferrous form when both substrate and molecular oxygen are present. This observation suggests an oxygen-mediated mechanism that enables electron transfer from electron-rich indole to haem iron. Such a reaction might involve the H76 and bring about a catalytically required conformational transition of the enzyme.

SUPPLEMENTARY DATA

Supplementary data are available at *JB* Online.

FUNDING

Grant-in-Aid for Young Scientists from MEXT (to H.S.). Grant-in-Aid for Scientific Research on Priority Areas from MEXT (to H.S. and Y.S.). Grant-in-Aid for Scientific Research from MEXT for Priority Area (Molecular Science for Supra Functional Systems, 20050029 and Structural Organization and Functional Mechanisms of Biological Macromolecular Assemblies, 20051026), Global Center of Excellence Program (Picobiology: Life Science at Atomic Level) and Targeted Protein Program (3D structural and functional analyses for elucidation of the mechanism of mitochondrial respiration) from MEXT (to T.O.).

CONFLICT OF INTEREST

None declared.

REFERENCES

1. Hayaishi, O. and Nozaki, M. (1969) Nature and mechanisms of oxygenases. *Science* **164**, 389–396
2. Feigelson, P. and Brady, F. O. (1974) *Molecular mechanism of oxygen activation*, Academic Press, New York
3. Hayaishi, O., Rothberg, S., Mehler, A. H., and Saito, Y. (1957) Studies on oxygenases; enzymatic formation of kynurenine from tryptophan. *J. Biol. Chem.* **229**, 889–896
4. Knox, W. E. and Mehler, A. H. (1950) The conversion of tryptophan to kynurenine in liver. I. The coupled tryptophan peroxidase-oxidase system forming formylkynurenine. *J. Biol. Chem.* **187**, 419–430
5. Yamamoto, S. and Hayaishi, O. (1967) Tryptophan pyrrolase of rabbit intestine. D- and L-tryptophan-cleaving enzyme or enzymes. *J. Biol. Chem.* **242**, 5260–5266
6. Muller, A. J. and Prendergast, G. C. (2007) Indoleamine 2,3-dioxygenase in immune suppression and cancer. *Curr. Cancer Drug Targets* **7**, 31–40
7. Takikawa, O. (2005) Biochemical and medical aspects of the indoleamine 2,3-dioxygenase-initiated L-tryptophan metabolism. *Biochem. Biophys. Res. Commun.* **338**, 12–19
8. Mellor, A. L. and Munn, D. H. (2004) IDO expression by dendritic cells: tolerance and tryptophan catabolism. *Nat. Rev. Immunol.* **4**, 762–774

9. Sono, M., Roach, M. P., Coulter, E. D., and Dawson, J. H. (1996) Heme-containing oxygenases. *Chem. Rev.* **96**, 2841–2888
10. Munn, D. H. and Mellor, A. L. (2007) Indoleamine 2,3-dioxygenase and tumor-induced tolerance. *J. Clin. Invest.* **117**, 1147–1154
11. Forouhar, F., Anderson, J. L., Mowat, C. G., Vorobiev, S. M., Hussain, A., Abashidze, M., Bruckmann, C., Thackray, S. J., Seetharaman, J., Tucker, T., Xiao, R., Ma, L. C., Zhao, L., Acton, T. B., Montelione, G. T., Chapman, S. K., and Tong, L. (2007) Molecular insights into substrate recognition and catalysis by tryptophan 2,3-dioxygenase. *Proc. Natl Acad. Sci. USA* **104**, 473–478
12. Feigelson, P. and Greengard, O. (1962) Regulation of liver tryptophan pyrrolase activity. *J. Biol. Chem.* **237**, 1908–1913
13. Britan, A., Maffre, V., Tone, S., and Drevet, J. R. (2006) Quantitative and spatial differences in the expression of tryptophan-metabolizing enzymes in mouse epididymis. *Cell Tissue Res.* **324**, 301–310
14. Miller, C. L., Llenos, I. C., Dulay, J. R., Barillo, M. M., Yolken, R. H., and Weis, S. (2004) Expression of the kynurenine pathway enzyme tryptophan 2,3-dioxygenase is increased in the frontal cortex of individuals with schizophrenia. *Neurobiol. Dis.* **15**, 618–629
15. Suzuki, S., Tone, S., Takikawa, O., Kubo, T., Kohno, I., and Minatogawa, Y. (2001) Expression of indoleamine 2,3-dioxygenase and tryptophan 2,3-dioxygenase in early concepti. *Biochem. J.* **355**, 425–429
16. Sedlmayr, P., Blaschitz, A., Wintersteiger, R., Semlitsch, M., Hammer, A., MacKenzie, C. R., Walcher, W., Reich, O., Takikawa, O., and Dohr, G. (2002) Localization of indoleamine 2,3-dioxygenase in human female reproductive organs and the placenta. *Mol. Hum. Reprod.* **8**, 385–391
17. Shimizu, T., Nomiyama, S., Hirata, F., and Hayaishi, O. (1978) Indoleamine 2,3-dioxygenase. Purification and some properties. *J. Biol. Chem.* **253**, 4700–4706
18. Hirata, F. and Hayaishi, O. (1972) New degradative routes of 5-hydroxytryptophan and serotonin by intestinal tryptophan 2,3-dioxygenase. *Biochem. Biophys. Res. Commun.* **47**, 1112–1119
19. Schutz, G., Killewich, L., Chen, G., and Feigelson, P. (1975) Control of the mRNA for hepatic tryptophan oxygenase during hormonal and substrate induction. *Proc. Natl Acad. Sci. USA* **72**, 1017–1020
20. Schimke, R. T., Sweeney, E. W., and Berlin, C. M. (1965) The Roles of Synthesis and Degradation in the Control of Rat Liver Tryptophan Pyrrolase. *J. Biol. Chem.* **240**, 322–331
21. Wagner, C. and Brown, A. T. (1970) Regulation of tryptophan pyrrolase activity in Xanthomonas pruni. *J. Bacteriol.* **104**, 90–97
22. Cho-Chung, Y. S. and Pitot, H. C. (1967) Feedback control of rat liver tryptophan pyrrolase. I. End product inhibition of trytophan pyrrolase activity. *J. Biol. Chem.* **242**, 1192–1198
23. Schutz, G., Chow, E., and Feigelson, P. (1972) Regulatory properties of hepatic tryptophan oxygenase. *J. Biol. Chem.* **247**, 5333–5337
24. Yoshida, T., Lorence, R. M., Choc, M. G., Tarr, G. E., Findling, K. L., and Fee, J. A. (1984) Respiratory proteins from the extremely thermophilic aerobic bacterium, Thermus thermophilus. Purification procedures for cytochromes c552, c555,549, and c1aa3 and chemical evidence for a single subunit cytochrome aa3. *J. Biol. Chem.* **259**, 112–123
25. Paul, K. G., Theorell, H., and Akeson, A. (1953) The molar light absorption of pyridine ferroprotoporphyrin (pyridine hemochromogen). *Acta Chem. Scand.* **7**, 1284–1287
26. Falk, J. E. (1964) Absorption spectra in *B.B.A. Library 2, Porphyrins and Metalloporphyrins*, pp. 231–246, Elsevier Publishing, Amsterdam
27. Ishimura, Y., Nozaki, M., and Hayaishi, O. (1970) The oxygenated form of L-tryptophan 2,3-dioxygenase as reaction intermediate. *J. Biol. Chem.* **245**, 3593–3602
28. Thackray, S. J., Bruckmann, C., Anderson, J. L., Campbell, L. P., Xiao, R., Zhao, L., Mowat, C. G., Forouhar, F., Tong, L., and Chapman, S. K. (2008) Histidine 55 of tryptophan 2,3-dioxygenase is not an active site base but regulates catalysis by controlling substrate binding. *Biochemistry* **47**, 10677–10684
29. Batabyal, D. and Yeh, S. R. (2007) Human tryptophan dioxygenase: a comparison to indoleamine 2,3-dioxygenase. *J. Am. Chem. Soc.* **129**, 15690–15701
30. Pant, K. C., Rogers, Q. R., and Harper, A. E. (1974) Plasma and tissue free amino acid concentrations in rats fed tryptophan-imbalanced diets with or without niacin. *J. Nutrition* **104**, 1584–1596
31. Hu, S., Smith, K. M., and Spiro, T. G. (1996) Assignment of Protoheme Resonance Raman Spectrum by Heme Labeling in Myoglobin. *J. Am. Chem. Soc.* **118**, 12638–12646
32. Rousseau, D. L., Ching, Y. C., Brunori, M., and Giacometti, G. M. (1989) Axial coordination of ferric Aplysia myoglobin. *J. Biol. Chem.* **264**, 7878–7881
33. Varadarajan, R., Lambright, D. G., and Boxer, S. G. (1989) Electrostatic interactions in wild-type and mutant recombinant human myoglobins. *Biochemistry* **28**, 3771–3781
34. Chen, Z., Ost, T. W., and Schelvis, J. P. (2004) Phe393 mutants of cytochrome P450 BM3 with modified heme redox potentials have altered heme vinyl and propionate conformations. *Biochemistry* **43**, 1798–1808
35. Dick, R., Murray, B. P., Reid, M. J., and Correia, M. A. (2001) Structure–function relationships of rat hepatic tryptophan 2,3-dioxygenase: identification of the putative heme-ligating histidine residues. *Arch. Biochem. Biophys.* **392**, 71–78
36. DeLano, W. L. (2002) *The PyMOL Molecular Graphics System* DeLano Scientific, San Carlos, CA, USA